

Density Functional Theory Study of Redox Pairs: 2. Influence of Solvation and Ion-Pair Formation on the Redox Behavior of Cyclooctatetraene and Nitrobenzene

Mu-Hyun Baik,[†] Cynthia K. Schauer,^{*†} and Tom Ziegler[‡]

Contribution from the Department of Chemistry, University of North Carolina, Chapel Hill, North Carolina 27599-3290, and Department of Chemistry, University of Calgary, Calgary, Alberta, Canada T2N 1N4

Received August 21, 2001

Abstract: A study of the electrochemical behavior of cyclooctatetraene (COT) and nitrobenzene with Density Functional Theory and the conductor like solvation model (COSMO) is reported. The two-electron reduction of the tub-shaped COT molecule is accompanied by a structural change to a planar structure of D_{4h} symmetry in the first electron addition step, and to a fully aromatic structure of D_{8h} symmetry in the second electron addition step. Theoretical models are examined that are aimed at understanding the electrolyte- and solvent-dependent redox behavior of COT, in which a single $2e^-$ redox wave is observed with KI electrolyte in liquid ammonia solution ($\Delta\Delta E(\text{disp}) = [E(-2) - E(-1)] - [E(-1) - E(0)] < 0$, inverted potential), while two $1e^-$ redox waves are observed ($\Delta\Delta E(\text{disp}) > 0$) with NR_4^+X^- ($\text{R} = \text{butyl, propyl}$; $\text{X}^- = \text{perchlorate}$) electrolyte in dimethylformamide solution. In all cases, the computed reaction energy profiles are in fair agreement with the experimental reduction potentials. A chemically intuitive theoretical square scheme method of energy partitioning is introduced to analyze in detail the effects of structural changes and ion-pair formation on the relative energies of the redox species. The structural relaxation energy for conversion of tub-COT to planar-COT is mainly apportioned to the first reduction step, and is therefore a positive contribution to $\Delta\Delta E(\text{disp})$. The effect of the structural change on the disproportionation energy for COT is counteracted by the substantially more positive reduction potential for planar-(COT)⁻¹ in comparison to tub-(COT)⁻¹. Ion pairing of alkali metal counterions with the anionic reduction products gives rise to a negative contribution to $\Delta\Delta E(\text{disp})$ because the second ion-pairing step is more exothermic than the first, and the reduction of [KA] ($\text{A} = \text{COT, NB}$) is more exothermic than the reduction of A^{-1} . For COT, this negative energy differential term as a result of ion pairing predicts the experimentally observed inversion in the two $1e^-$ potentials ($\Delta\Delta E(\text{disp}) < 0$). Nitrobenzene is treated with the same computational protocol to provide a system for comparison that is not complicated by the major structural change that influences the COT energy profile.

Introduction

The electronic structure and chemical behavior of cyclooctatetraene (COT) has attracted experimental and theoretical attention since it was proposed as an example of a hydrocarbon ring displaying Hückel antiaromaticity with 8 π -electrons.¹ A few aspects of COT that have been studied include the interchange of single and double bonds,² ring inversion,³ the use of COT as a ligand for transition metal complexes,⁴ and the reductive electrochemistry of COT,^{5,6} which is the main focus of this work. In agreement with the predictions of Hückel

theory, doubly reduced (COT)⁻² is an aromatic system, and the reduction is accompanied by a structural change of the tub-shaped neutral molecule to a planar ring of D_{8h} symmetry.

Cyclooctatetraene, under select environmental conditions, is a member of a class of molecules that display a so-called "inverted" order of potentials characterized by a second reduc-

* Corresponding author. E-mail: schauer@unc.edu.

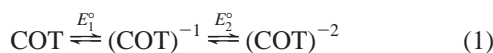
[†] University of North Carolina.

[‡] University of Calgary.

(1) (a) Hückel, E. *Grundzüge der Theorie ungesättigter und aromatischer Verbindungen*; Verlag Chemie: Berlin, Germany, 1938. (b) Skancke, A.; Hosmane, R. S.; Liebman, J. F. *Acta Chem. Scand.* **1998**, *52*, 967–974. (c) Politzer, P.; Murray, J. S.; Seminario, J. M. *Int. J. Quantum Chem.* **1994**, *50*, 273–277. (d) Trindle, C. *Int. J. Quantum Chem.* **1998**, *67*, 367–376. (e) Glukhovtsev, M. N.; Bach, R. D.; Laiter, S. J. *Mol. Struct. (THEOCHEM)* **1997**, *417*, 123–129. (f) Murray, J. S.; Seminario, J. M.; Politzer, P. *Int. J. Quantum Chem.* **1994**, *49*, 575–579. (g) von Schleyer, P., Ed. *Aromaticity: Chem. Rev.* **2001**, *101*, 1115–1566. (h) Klärner, F. G. *Angew. Chem., Int. Ed.* **2001**, *40*, 3977–3981.

(2) (a) Oth, J. F. M. *Pure Appl. Chem.* **1971**, *25*, 573–622. (b) Paquette, L. A.; Wang, T.-Z.; Luo, J.; Cottrell, C. E.; Clough, A. E.; Anderson, L. B. *J. Am. Chem. Soc.* **1990**, *112*, 239–253. (c) Anet, F. A. L. *J. Am. Chem. Soc.* **1962**, *84*, 671–672. (d) Paquette, L. A.; Trova, M. P.; Luo, J.; Clough, A. E.; Anderson, L. B. *J. Am. Chem. Soc.* **1990**, *112*, 228–239. (e) Staley, S. W.; Grimm, R. A.; Sablosky, R. A. *J. Am. Chem. Soc.* **1998**, *120*, 3671–3674. (f) Staley, S. W.; Kehlbeck, J. D.; Grimm, R. A.; Sablosky, R. A.; Boman, P.; Eliasson, B. *J. Am. Chem. Soc.* **1998**, *120*, 9793–9799. (g) Stevenson, C. D.; Kim, Y. S. *J. Am. Chem. Soc.* **2000**, *122*, 3211–3215. (h) Boman, P.; Eliasson, B.; Grimm, R. A.; Martin, G. S.; Strnad, J. T.; Staley, S. W. *J. Am. Chem. Soc.* **1999**, *121*, 1558–1564. (i) Staley, S. W.; Grimm, R. A.; Boman, P.; Eliasson, B. *J. Am. Chem. Soc.* **1999**, *121*, 7182–7187. (j) Staley, S. W.; Vignon, S. A.; Eliasson, B. *J. Org. Chem.* **2001**, *66*, 3871–3877. (k) Boman, P.; Eliasson, B.; Grimm, R. A.; Staley, S. W. *J. Chem. Soc., Perkin Trans. 2* **2001**, 1130–1138. (l) Baldrige, K. K.; Siegel, J. S. *J. Am. Chem. Soc.* **2001**, *123*, 1755–1759. (m) Baldrige, K. K.; Siegel, J. S. *J. Am. Chem. Soc.* **2002**, *124*, 5514–5517. (3) (a) Anet, F. A. L.; Bourn, A. J. R.; Lin, Y. S. *J. Am. Chem. Soc.* **1964**, *86*, 3576–3577. (b) Ermer, O.; Klärner, F.-G.; Wette, M. *J. Am. Chem. Soc.* **1986**, *108*, 4908–4911. (c) Parquette, L. A.; Wang, T.-Z.; Cottrell, C. E. *J. Am. Chem. Soc.* **1987**, *109*, 3730–3734.

tion potential that is thermodynamically more favorable than the first.⁷ The reduction of COT (eq 1) has been studied by



using electrochemical methods, including cyclic voltammetry (CV)^{5e} and ac/dc polarography (AC-P/DC-P).^{5a,g} A planar structure of the monoanion has been established by spectroscopic methods,^{5b} indicating that the main structural rearrangement is connected to the first reduction step. The electrochemical behavior of COT has caused some discussion in the literature⁷ mainly due to its electrolyte dependence. If the electrolyte used in the experiment contains noncoordinating cations such as NR₄⁺ (R = butyl, propyl), two distinct reduction waves are observed,^{5a,d} whereas in the presence of coordinating cations such as K⁺, a single 2e⁻ reduction wave results.^{5c} A single 2e⁻ reduction arises because the 1e⁻ reduced intermediate is unstable with respect to disproportionation (eq 2). Allendoerfer and Rieger,^{5a} Katz,^{5b}



Smith and Bard,^{5e} Smentowski and Stevenson,^{6a-f} and others^{5,6} have provided convincing experimental evidence that the right side of the equilibrium (eq 2) is favored if the counteranion B⁺ is a potassium cation, which forms mono- and dipotassium ion pairs with (COT)⁻¹ and (COT)⁻² anions, respectively. The free solvated (COT)⁻¹ is thermodynamically stable with respect to disproportionation.

A few theoretical studies have been reported on COT, including investigations directed at understanding its electrochemical behavior. Dewar used semiempirical calculations in the gas phase,^{8a} and others have applied more sophisticated methods^{8b-d} to compute the relative energies of the redox species. A very poor agreement with experiment was uniformly found, demonstrating the limited value of these gas-phase models for the investigation of the electrochemical behavior in solution. Recently, Evans and Hu employed a combination of AM1 calculations and estimates of the solvation energy based

on the Born model to predict disproportionation constants for a variety of organic systems, including COT, with good success.^{7e} Considerable theoretical efforts^{8e-o} have also been inspired by the single bond–double bond interchange and ring inversion, leading to a thorough theoretical characterization of COT. The electrolyte-dependent electrochemical behavior of COT has not been addressed theoretically.

In this paper, we present a complete theoretical model for the disproportionation reaction of COT as solvated ions and solvated ion pairs based on Density Functional Theory (DFT)⁹ calculations coupled self-consistently to a continuum solvation model.¹⁰ Our model predicts that the disproportionation is energetically downhill for the ion pairs and uphill for the solvated anions. The calculated energy differences are compared to experimental redox potentials. Furthermore, a new energy-partitioning scheme is presented that allows deconvolution of the relative energies for the different redox products into chemically intuitive partial energies. To contrast the behavior of COT, we have carried out calculations that examine the electrochemical behavior of nitrobenzene, which displays two well-separated 1e⁻ waves under all environmental conditions in dipolar aprotic solvents.¹¹

Computational Details

DMol. The nonlocal functionals suggested by Becke^{12a} (exchange) and Lee–Yang–Parr^{12b} (correlation) [BLYP] were employed self-consistently for the full geometry optimization using the DMol3^{13a} program package. A set of “double numerical plus” (DNP) basis functions with a FINE mesh was used throughout the study and all electrons were included (no frozen core).

- (4) (a) Edwin, J.; Geiger, W. E. *J. Am. Chem. Soc.* **1990**, *112*, 7104–7112. (b) Geiger, W. E.; Rieger, P. H.; Corbato, C.; Edwin, J.; Fonseca, E.; Lane, G. A.; Mevs, J. M. *J. Am. Chem. Soc.* **1993**, *115*, 2314–2323. (c) Rathore, R.; Lindeman, S. V.; Kumar, A. S.; Kochi, J. K. *J. Am. Chem. Soc.* **1998**, *120*, 6931–6939.
- (5) (a) Allendoerfer, R. D.; Rieger, P. H. *J. Am. Chem. Soc.* **1965**, *87*, 2336–2344. (b) Katz, T. J. *J. Am. Chem. Soc.* **1960**, *82*, 3784–3785. (c) Paquette, L. A.; Wright, D., III; Traynor, S. G.; Taggart, D. L.; Ewing, G. D. *Tetrahedron* **1976**, *32*, 1885–1891. (d) Lehmkuhl, H.; Kintopf, S.; Janssen, E. *J. Organomet. Chem.* **1973**, *56*, 41–52. (e) Smith, W. H.; Bard, A. J. *J. Electroanal. Chem.* **1977**, *76*, 19–26. (f) Thielen, D. R.; Anderson, L. B. *J. Am. Chem. Soc.* **1972**, *94*, 2521–2523. (g) Huebert, B. J.; Smith, D. E. *J. Electroanal. Chem.* **1971**, *31*, 333–348.
- (6) (a) Smentowski, F. J.; Stevenson, G. R. *J. Am. Chem. Soc.* **1967**, *89*, 5120–5123. (b) Smentowski, F. J.; Stevenson, G. R. *J. Am. Chem. Soc.* **1968**, *90*, 4661–4662. (c) Smentowski, F. J.; Owens, R. M.; Faubion, B. D. *J. Am. Chem. Soc.* **1968**, *90*, 1537–1540. (d) Smentowski, F. J.; Stevenson, G. R. *J. Phys. Chem.* **1969**, *73*, 340–345. (e) Smentowski, F. J.; Owens, R. M.; Faubion, B. D. *J. Am. Chem. Soc.* **1969**, *91*, 7401–7404. (f) Stevenson, G. R.; Concepcion, J. G. *J. Phys. Chem.* **1972**, *76*, 2176–2178. (g) Strauss, H. L.; Katz, T. J.; Fraenkel, G. K. *J. Am. Chem. Soc.* **1963**, *85*, 2360–2364. (h) Farrel, P. G.; Mason, S. F. *Z. Naturforsch.* **1961**, *16b*, 848–849. (i) Ohno, M.; von Niessen, W.; Pairaud, E.; Heinesch, J.; Delwiche, J. *J. Electron Spectrosc. Relat. Phenom.* **1995**, *73*, 261–270. (j) Percec, M. *Spectrochim. Acta* **1991**, *47A*, 799–809. (k) Dvorak, V.; Michl, J. *J. Am. Chem. Soc.* **1976**, *98*, 1080–1086.
- (7) For discussions of multielectron electrochemistry see: (a) Gennett, T.; Geiger, W. E.; Willet, B.; Anson, F. C. *J. Electroanal. Chem.* **1987**, *222*, 151–160. (b) Fernandes, J. B.; Zhang, L. Q.; Schultz, F. A. *J. Electroanal. Chem.* **1991**, *297*, 145–161. (c) Hinkelmann, K.; Heinze, J. *Ber. Bunsenges. Phys. Chem.* **1987**, *91*, 243–249. (d) Bowyer, W. J.; Geiger, W. E. *J. Electroanal. Chem.* **1988**, *239*, 253–271. (e) Evans, D. H.; Hu, K. *J. Chem. Soc., Faraday Trans.* **1996**, *92*, 3983–3990. (f) Evans, D. H.; Lehmann, M. W. *Acta Chem. Scand.* **1999**, *53*, 765–774.
- (8) (a) Dewar, M. J.; Harget, A.; Haselbach, E. *J. Am. Chem. Soc.* **1969**, *91*, 7521–7523. (b) Hrovat, D. A.; Hammons, J. H.; Stevenson, C. D.; Borden, W. T. *J. Am. Chem. Soc.* **1997**, *119*, 9523–9526. (c) Zuilhof, H.; Lodder, G. *J. Phys. Chem.* **1995**, *99*, 8033–8037. (d) Kato, S.; Lee, H.-S.; Gareyev, R.; Wenthhold, P. G.; Lineberger, W. C.; DePuy, C. H.; Bierbaum, V. M. *J. Am. Chem. Soc.* **1997**, *119*, 7863–7864. (e) Andres, J. L.; Castano, O.; Morreale, A.; Palmeiro, R.; Gomperts, R. *J. Chem. Phys.* **1998**, *108*, 203–207. (f) Trindle, C.; Wolfskill, T. *J. Org. Chem.* **1991**, *56*, 5426–5436. (g) Zhou, X.; Liu, R.; Pulay, P. *Spectrochim. Acta* **1993**, *49A*, 953–964. (h) Karadakov, P. B.; Gerratt, J.; Cooper, D. L.; Raimondi, M. *J. Phys. Chem.* **1995**, *99*, 10186–10195. (i) Dewar, M. J.; Merz, K. M., Jr. *J. Phys. Chem.* **1985**, *89*, 4739–4744. (j) Hammons, J. H.; Hrovat, D. A.; Borden, W. T. *J. Am. Chem. Soc.* **1991**, *113*, 4500–4505. (k) Hrovat, D. A.; Borden, W. T. *J. Am. Chem. Soc.* **1992**, *114*, 5879–5881. (l) Hrovat, D. A.; Borden, W. T. *J. Mol. Struct. (THEOCHEM)* **1997**, *398–399*, 211–220. (m) Kato, S.; Gareyev, R.; DePuy, C. H.; Bierbaum, V. M. *J. Am. Chem. Soc.* **1998**, *120*, 5033–5042. (n) Stevenson, C. D.; Brown, E. C.; Hrovat, D. A.; Borden, W. T. *J. Am. Chem. Soc.* **1998**, *120*, 8864–8867. (o) Hammons, J. H.; Hrovat, D. A.; Borden, W. T. *J. Am. Chem. Soc.* **1991**, *113*, 4500–4505. (p) Kelterer, A. M.; Landgraf, S.; Grampp, G. *Spectrochim. Acta A-Mol. Biomolec. Spectrosc.* **2001**, *57*, 1959–1969. (q) Sommerfeld, T. *J. Am. Chem. Soc.* **2002**, *124*, 1119–1124.
- (9) (a) Parr, R. G.; Yang, W. *Density Functional Theory of Atoms and Molecules*; Oxford University Press: New York, 1989. (b) Ziegler, T. *Chem. Rev.* **1991**, *91*, 651–667.
- (10) For a review of continuum solvation models see for example: (a) Tomasi, J.; Persico, M. *Chem. Rev.* **1994**, *94*, 2027–2094. (b) Cramer, C. J.; Truhlar, D. G. In *Solvent Effects and Chemical Reactivity*; Tapia, O., Bertran, J., Eds.; Kluwer Academic Publishers: Hingham, MA, 1996; pp 1–80. (c) Cramer, C. J.; Truhlar, D. G. *Chem. Rev.* **1999**, *99*, 2161–2200.
- (11) (a) Smith, W. H.; Bard, A. J. *J. Am. Chem. Soc.* **1975**, *97*, 5203–5210. (b) Holleck, L.; Becher, D. *J. Electroanal. Chem.* **1962**, *4*, 321–331. (c) Symons, M. C. R. *J. Phys. Chem.* **1967**, *71*, 172–183. (d) Jensen, B. S.; Parker, V. D. *J. Chem. Soc., Chem. Commun.* **1974**, *10*, 367–368.
- (12) (a) Becke, A. D. *Phys. Rev. A* **1988**, *38*, 3098–3100. (b) Lee, C.; Yang, W.; Parr, R. G. *Phys. Rev. B* **1988**, *37*, 785–789.
- (13) (a) Delly, B. *J. Chem. Phys.* **1990**, *92*, 508–517. (b) DMol3; Molecular Simulations Inc.: San Diego, CA, 1997 (c) ADF 1999; Baerends, E. J.; Bérces, A.; Bo, C.; Boerrigter, P. M.; Cavallo, L.; Deng, L.; Dickson, R. M.; Ellis, D. E.; Fan, L.; Fischer, T. H.; Fonseca Guerra, C.; van Gisbergen, S. J. A.; Groeneveld, J. A.; Gritsenko, O. V.; Harris, F. E.; van den Hoek, P.; Jacobsen, H.; van Kessel, G.; Kootstra, F.; van Lenthe, E.; Osinga, V. P.; Philipsen, P. H. T.; Post, D.; Pye, C. C.; Ravenek, W.; Ros, P.; Schipper, P. R. T.; Schreckenbach, G.; Snijders, J. G.; Sola, M.; Swerhone, D.; te Velde, G.; Vernooijs, P.; Versluis, L.; Visser, O.; van Wezenbeek, E.; Wiesenekker, G.; Wolff, S. K.; Woo, T. K.; Ziegler, T.

ADF. In ADF^{13c,d} calculations, a triple- ζ STO basis set was utilized, with one set of polarization functions as provided in the package (basis set IV, comparable to 6-311G*), together with the BLYP functional.¹² All electrons were included in the calculation (no frozen core) employing the unrestricted spin formalism for all calculations.

COSMO. Solvation effects have been included by using the conductor-like screening model (COSMO) suggested by Klamt and Schüürmann^{14a} and implemented in DMol by Andzelm and Klamt^{14b} and in ADF by Pye and Ziegler.^{14c} The crucial part of the solvation calculation is the choice of radii that defines the cavity representing the solute. In DMol calculations, the Klamt surface is used, whereas in ADF calculations, the solvent-excluding surface was chosen. The standard radii provided with the package were used in DMol calculations (C, 1.53 Å; H, 1.08 Å; K, 2.39 Å; N, 1.83 Å; O, 1.72 Å). Due to its recent implementation, standard COSMO radii for ADF are not routinely available. The radii suggested by Pye and Ziegler^{14c} were used with an estimated value for potassium (C, 2.30 Å; H, 1.16 Å; K, 2.95 Å; N, 1.4 Å; O, 1.4 Å). A direct comparison of the calculated absolute solvation energies is problematic if different surfaces and radii are used in addition to different charge distribution schemes. For charged species, the dominant term is the monopole term inside the surface and the sphere sizes are less important. Only a moderate agreement of the solvation energies between the two DFT packages is expected. In accordance with the experiments we have used the dielectric constant of dimethylformamide^{5a,11d} (DMF, $\epsilon = 36.7$) for the solvated ion model and that of liquid ammonia^{5c,11a} ($\epsilon = 25.0$) for the solvated ion-pair model.

Vibrational Frequencies. The vibrational frequencies of all three oxidation states in the gas-phase, solvated ions, and solvated ion-pairs models were calculated for both cyclooctatetraene and nitrobenzene by double numerical differentiation of the analytical energy gradient, using the nonlocal density functionals (BLYP) and the finite-difference method. The unscaled vibrational energies were then used to calculate the entropy correction terms at 298.15 and 250 K, using the common approximations (ideal gas, rigid rotor, and harmonic oscillator) for the partition functions. Thermal corrections for the electronic energy are neglected. Due to computational demands these calculations were only carried out with DMol3 and the computed corrections were applied to both DMol3 and ADF energies. We note that the vibrational entropy correction terms obtained with gas-phase and COSMO models differ significantly. The COSMO results are in better agreement with experimental observations, indicating that it is inappropriate to use the gas-phase vibrational corrections for the COSMO model.¹⁵

Results and Discussion

Structural Parameters for Cyclooctatetraene (COT) Reduction. The structure of monoanionic COT has been the subject of numerous theoretical and experimental studies. Hammons and co-workers^{8j} have reported high-level ab initio calculations and have given a firm theoretical foundation for the spectroscopically supported¹⁶ planar structure of D_{4h} symmetry for the monoanion. The frontier orbitals of neutral COT are shown in Figure 1, and the results of gas-phase calculations are sum-

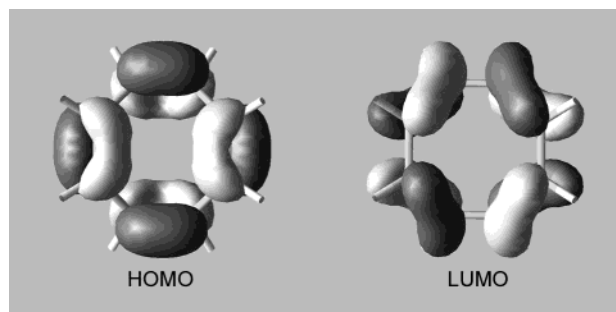


Figure 1. HOMO and LUMO of cyclooctatetraene.

Table 1. Gas-Phase Energies of (COT)^{0/-1/-2} and First and Second Adiabatic Electron Attachment Energies

(a) Gas-Phase Energies of (COT) ^{0/-1/-2}			
	COT	(COT) ⁻¹	(COT) ⁻²
DMol3			
enthalpy H/au	-309.562	-309.589	-309.44
ZPE/eV	3.485	3.432	3.316
entropy S/eu	81.82	81.61	82.13
$-T\Delta S$ at 298.15 K/eV	-1.198	-1.056	-1.207
ADF			
binding energy/eV	-94.310	-95.140	-91.441
(b) First and Second Adiabatic Electron Attachment Energies			
	(0) \rightarrow (-1)	(-1) \rightarrow (-2)	$\Delta\Delta E(\text{disp})$
ΔH (eV) – DMol	-0.735	3.955	4.690
ΔG (eV) – DMol	-0.645 (-0.58) ^a	3.689	4.334
ΔH (eV) – ADF	-0.830	3.696	4.526
ΔG (eV) – ADF	-0.741 (-0.58) ^a	3.430	4.171

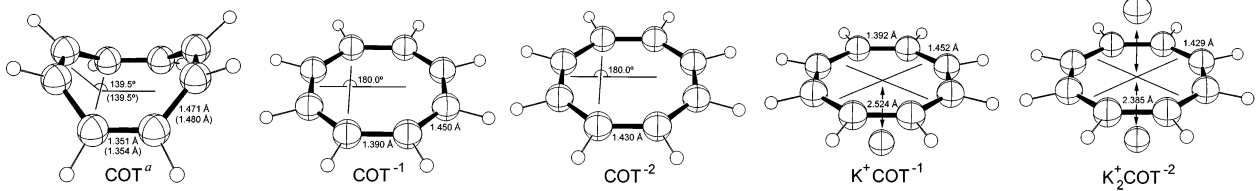
^a Experimental value taken from ref 17a.

marized in Table 1. The highest occupied molecular orbital (HOMO) is an in-phase π -interaction between the shorter C–C bonds and the LUMO is the corresponding out-of-phase combination. The observed structural change is intuitively understandable if the lowest unoccupied molecular orbital (LUMO) of the neutral molecule is considered. This unoccupied orbital is skewed due to the tub-shape of COT, which results in poor overlap of the in-phase p-p interactions between the longer C–C bonds. The occupation of this orbital in the first reduction step is the main driving force for the observed structural change. By adopting a planar structure, the in-phase overlap of the p-orbitals along the longer C–C bond becomes significantly more favorable. The D_{4h} structure of the monoanion, with two different carbon–carbon bond lengths, is the result of a first-order Jahn–Teller distortion. The addition of a second electron leads to an aromatic 10 π -electron system, in which all carbon–carbon distances are equal. Previously reported gas-phase bond lengths and angles from high-level ab initio calculations⁸ are well reproduced in our calculations, and the gas-phase structures will not be discussed further.

To model the electrochemical experiments for the solvated ions and ion pairs, calculations including the COSMO solvation correction were carried out for $\epsilon = 36.7$ (DMF) for COT, (COT)⁻¹, and (COT)⁻² and $\epsilon = 25.0$ (NH₃) for COT, [K(COT)], and [K₂(COT)]. Starting from the gas-phase geometries, the structure of the neutral and both ionic species and the ion pairs were reoptimized with COSMO corrections, and the metric parameters are presented in Table 2. The solvation geometries for the COT rings, including those for the ion pairs, only differ slightly from the gas-phase structures. The Cartesian coordinates

- (14) (a) Klamt, A.; Schüürmann, G. *J. Chem. Soc., Perkin Trans.* **1993**, 2, 799–805. (b) Andzelm, J.; Koelmel, C.; Klamt, A. *J. Chem. Phys.* **1995**, 103, 9312–9320. (c) Pye, C.; Ziegler, T. *Theor. Chem. Acc.* **1999**, 101, 396–408.
- (15) (a) Olivares del Valle, F. J.; Tomasi, J. *Chem. Phys.* **1987**, 114, 231–239. (b) Olivares del Valle, F. J.; Aguilar, M.; Tolosa, S.; Contrador, J. C.; Tomasi, J. *Chem. Phys.* **1990**, 143, 371–379. (c) Olivares del Valle, F. J.; Tomasi, J. *Chem. Phys.* **1991**, 150, 139–150. (d) Aguilar, M. A.; Olivares del Valle, F. J.; Tomasi, J. *Chem. Phys.* **1991**, 150, 151–161. (e) Banacký, P.; Zajac, A. *Chem. Phys.* **1988**, 123, 267–276. (f) Banacký, P.; Zajac, A. *Chem. Phys.* **1989**, 130, 241–255. (g) See Supporting Information for both results and a few comments on this issue.
- (16) (a) Kimmel, P. I.; Strauss, H. L. *J. Phys. Chem.* **1968**, 72, 2813–2817. (b) Wenthold, P. G.; Hrovat, D. A.; Borden, W. T.; Lineberger, W. C. *Science* **1996**, 272, 1456–1459.

Table 2. COSMO Structures and Energies



	COT $\epsilon = 37.5$	(COT) ⁻¹ $\epsilon = 37.5$	(COT) ⁻² $\epsilon = 37.5$	COT $\epsilon = 25.0$	[K(COT)] $\epsilon = 25.0$	[K ₂ (COT)] $\epsilon = 25.0$
DMol3						
total E^b	-309.54	-309.65	-309.75	-309.54	-909.54	-1509.55
LUMO ^c	-2.33	0.53	0.88	-2.33	-0.32	-0.34
HOMO ^d	-5.07	-2.99	-2.11	-5.07	-3.52	-3.12
$E(\text{sol.v.})^e$	-3.82	-51.65	-191.19	-3.81	-18.44	-10.16
ADF						
binding E^f	-94.401	-97.338	-99.538	-94.404	-96.095	-97.996
LUMO ^c	-2.32	0.13	0.37	-2.37	-1.02	-0.77
HOMO ^d	-5.06	-2.75	-1.70	-5.03	-3.44	-3.01
$E(\text{sol.v.})^e$	-4.78	-54.41	-192.76	-4.77	-15.25	-8.06

^a Structural features of the neutral COT in liquid ammonia are given in parentheses. ^b Total SCF energy in au. ^c Lowest unoccupied molecular orbital energy in eV; as a result of the unrestricted formalism the LUMO of the doublet (COT)⁻¹ and [K(COT)] are technically the β -spin-orbitals of the highest occupied orbitals. To allow comparison with the LUMO energies of (COT)⁻² and [K₂(COT)] the energies of the empty orbital with the same spin are given. ^d Highest occupied molecular orbital energy in eV. ^e Electrostatic solvation energy in kcal/mol. ^f Binding energy in eV: ADF computes binding energies rather than the absolute SCF energies, which are defined as the total molecular energy minus the sum of the atomic fragment energies.

of all structures are given as Supporting Information. In [K(COT)] and [K₂(COT)], the distances between the potassium ion and the centroid of the COT ring are 2.52 and 2.39 Å, respectively.

Energetics of COT Reduction. The energy of the disproportionation reaction will be calculated for the gas-phase, solvated ion, and ion-pair models. The free energy changes, ΔG , for the redox reactions will be used to construct a realistic model of the disproportionation reaction, which requires the addition of the entropic energy terms at a given temperature to the standard electronic enthalpies. In addition, the zero-point energy (ZPE), which could change upon reduction and introduce another differential energy term to the total electron attachment energy, must also be added.

(a) Gas-Phase Results. The electronic enthalpies of the three oxidation states in gas phase, ZPE corrections and entropic terms are given in Table 1. The first electron attachment energy can be computed as the energy difference between the neutral and anionic species. If only the electronic enthalpies are considered, the first electron attachment energy in gas phase is calculated to be -0.74 eV (DMol3)/-0.83 eV (ADF). Addition of zero-point energy and entropic terms at 298K shift the calculated energies to -0.65 eV (DMol3)/-0.74 eV (ADF), which are in good agreement with the experimental value of -0.58 ± 0.10 eV.^{17a}

The net change in electronic energy $\Delta\Delta E(\text{disp})$ for the disproportionation is given by

$$\Delta\Delta E(\text{disp}) = [E(-2) - E(-1)] - [E(-1) - E(0)] \quad (3)$$

where E is the energy of the neutral, monoanionic, and dianionic forms of the complex, respectively.¹⁸ A negative $\Delta\Delta E(\text{disp})$ value indicates a net stabilization for the reaction, and occurs

when more energy is released in the second reduction step than the first. The relative energies of the three species involved in the disproportionation reaction are compared in Figure 2. In agreement with previously reported studies by Dewar and others,⁸ the gas-phase calculation indicates an energetically stable monoanion with respect to the disproportionation reaction. The corresponding energy differences of the two half reactions of the disproportionation and their sum are given in Table 1b. A total reaction enthalpy of +4.7 eV (DMol)/+4.5 eV (ADF) is in fair agreement with Dewar's MNDO/2 calculation, which predicted a reaction enthalpy of +3.96 eV.^{8a}

(b) Solvated Ion and Solvated Ion-Pair Models. Introducing solvation has a small effect on the energy of neutral COT, whereas the mono- and dianion are stabilized by -54 and -193 kcal/mol, respectively, in DMF solution (Table 2). The first electron attachment energy in solution is computed as -3.12 eV (DMol)/-2.94 eV (ADF), while the second is computed as -2.71 eV (DMol)/-2.20 eV (ADF). The energy for the disproportionation reaction, $\Delta\Delta E(\text{disp})$, is therefore +0.41 eV (DMol)/+0.74 eV (ADF), which is thermodynamically uphill. If the ZPE and entropic terms are included, the reaction free energy at room temperature is computed as +0.38 eV (DMol)/+0.70 eV (ADF).

The relative energies of COT and the ion pairs [K(COT)] and [K₂(COT)] have been used to evaluate the energy of the disproportionation reaction given in eq 2. The dielectric constant of liquid ammonia ($\epsilon = 25.0$) has been used for the ion pair model. As the energy profile shown in Figure 2b indicates, the $\Delta\Delta E(\text{disp})$ value for the ion-pair system is negative, indicating that the disproportionation reaction is energetically downhill. If only electronic enthalpies are considered, the overall reaction

(17) (a) Denault, J. W.; Chen, G.; Cooks, R. G. *J. Am. Soc. Mass Spectrom.* **1998**, *9*, 1141–1145. (b) Wentworth, W. E.; Ristau, W. *J. Phys. Chem.* **1969**, *73*, 2126–2133. (c) Stevenson, G. R.; Forch, B. E. *J. Phys. Chem.* **1981**, *85*, 378–382.

(18) In ADF the molecular energies are routinely computed as binding energies, which are defined as the total energy minus the sum of atomic fragment energies, where spherically symmetric restricted atom fragments are assumed. Since we are only interested in energy differences the ADF binding energies can be used instead of the total energy.

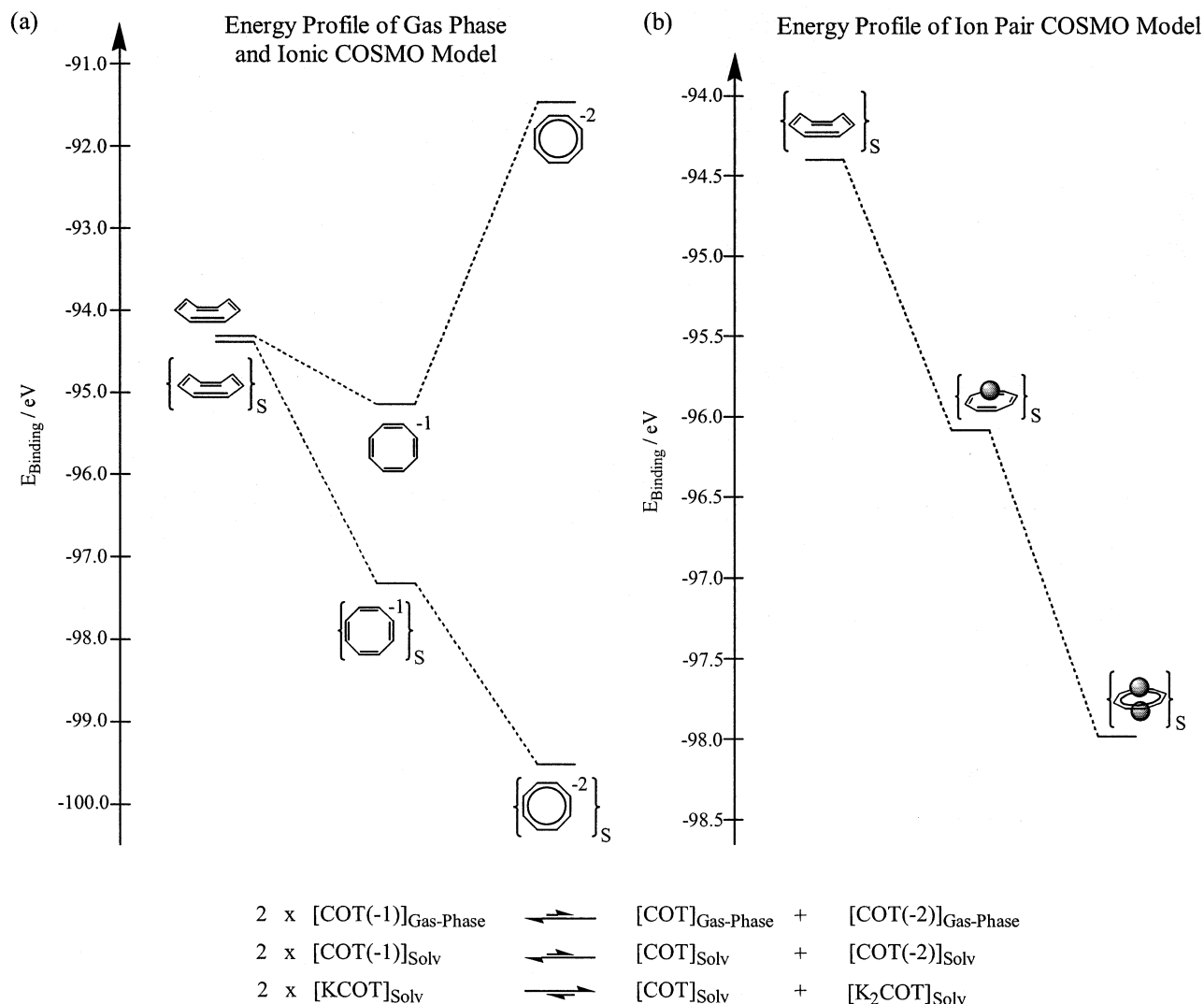


Figure 2. Total binding energies (ADF results) of the three redox states of cyclooctatetraene for gas phase, solvated ion, and solvated ion-pair models.

Table 3. Calculated Reduction Potentials Based on Electronic Enthalpy Only ($E^\circ(\Delta H)$) and the Gibbs Free Energy ($E^\circ(\Delta G)$) for COT^a and Experimental Reduction Potentials (in V) vs SHE

	(a) Calculated Reduction Potentials					
	(0) → (-1)		(-1) → (-2)		$E_1^\circ - E_2^\circ = \Delta\Delta E(\text{disp})$	
	$\Delta E_1/E_1^\circ(\Delta H)$	$\Delta E_1/E_1^\circ(\Delta G)$	$\Delta E_2/E_2^\circ(\Delta H)$	$\Delta E_2/E_2^\circ(\Delta G)$	ΔH	ΔG
DMol3						
solv. ion (DMF)	-3.12/-1.31	-3.16/-1.27	-2.71/-1.72	-2.78/-1.65	0.41	0.38
solv. ion pair (NH ₃)	-3.65	-3.79	-3.91	-3.95	-0.26	-0.16
ADF						
solv. ion (DMF)	-2.94/-1.49	-2.97/-1.46	-2.20/-2.23	-2.27/-2.16	0.74	0.70
solv. ion pair (NH ₃)	-1.69	-1.84	-1.90	-1.95	-0.21	-0.11
	(b) Experimental Reduction Potentials					
experimental	E_1° (0) → (-1)	E_2° (-1) → (-2)	$E_1^\circ - E_2^\circ$			
solv. ion (DMF) ^b	-1.38	-1.62	0.24			
solv. ion pair (NH ₃) ^c	-1.41	-1.19	-0.22			

^a In DMol3, we have added the SCF energy of the solvated K⁺ ion on the reactant side for the reaction $\text{COT}^0 + \text{K}^+ + \text{e}^- \rightarrow [\text{K}(\text{COT})]$ and $[\text{K}(\text{COT})] + \text{K}^+ + \text{e}^- \rightarrow [\text{K}_2(\text{COT})]$. In ADF, this correction is not necessary, since the binding energies are computed and the energies are all normalized to the sum of the fragment energies. Therefore ADF results are referenced to the reaction $\text{COT}^0 + \text{K}^0 \rightarrow [\text{K}(\text{COT})]$ and $[\text{K}(\text{COT})] + \text{K}^0 \rightarrow [\text{K}_2(\text{COT})]$. ^b Reference 5a. ^c Reference 5e.

$\Delta\Delta E(\text{disp})$ value for the solvated ion pair system is -0.26 eV (DMol)/ -0.21 eV (ADF), and, including the ZPE and entropy corrections at 250 K, -0.16 eV (DMol)/ -0.11 eV (ADF) (Table 3a).

(c) Comparison to Experimental Redox Potentials. The electron attachment energies discussed above are absolute potentials for the reduction. Since experimental data are always reported relative to a reference, the absolute potential of the

reference electrode must be added to relate these absolute numbers to experimental electrochemical data. An absolute potential of 4.43 eV has been measured for the standard hydrogen electrode (SHE),^{19a} which has been used widely to correlate computed redox potentials to experimentally measured redox potentials.^{19b–p} With this correction, the first reduction energy is 1.31 eV (DMol)/1.49 eV (ADF) vs SHE. Using eq 4 (n = number of electrons involved in the redox process; F = Faraday constant) the computed first reduction potential is

$$E^\circ = -\Delta G^\circ/nF \quad (4)$$

−1.31 V (DMol)/−1.49 V (ADF). This reduction potential is in good agreement with the experimental value of −1.38 V²⁰ reported by Allendoerfer and Rieger.^{5a} The addition of the ZPE and entropy corrections has a very minor effect of 30–40 mV, and the corrected redox potential is −1.27 V (DMol)/−1.46 V (ADF). The second reduction potential E°_2 is computed as −1.72 V (DMol)/−2.23 V (ADF), using only the electronic enthalpy and −1.65 V (DMol)/−2.16 V (ADF) including ZPE and entropy corrections, where −1.62 V has been reported experimentally.^{5a} If the ZPE and entropic terms are included, the reaction free energy for the disproportionation reaction at room temperature is computed as +0.38 eV (DMol)/+0.70 eV (ADF). The DMol3 results agree fairly well with the experimental value of 0.24 eV,^{5a} but the deviation of the ADF result is quite large. The experimental and calculated redox potentials are summarized in Table 3.

Assuming rapid electron-transfer kinetics, a single 2e[−] reduction would be observed at the average of the two 1e[−] potentials for a case like the solvated ion pair model, for which a thermodynamically downhill disproportionation reaction is predicted. The corrected $\Delta\Delta E(\text{disp})$ value for the solvated ion pair system of −0.16 eV (DMol)/−0.11 eV (ADF) is in good agreement with the $\Delta E_{1/2}$ value²¹ of −0.22 eV estimated from a digital voltammogram simulation by Smith and Bard.^{5c}

Although it would be of interest to compare the 1e[−] potential for the solvated ion-pair model with the solvated ion model, the individual potentials E°_1 and E°_2 are not meaningful for the ion-pair model for primarily two reasons. First, to accurately

evaluate the absolute potential for the reaction, $[\text{K}^+]_{\text{Solv}} + \text{e}^- + [\text{COT}]_{\text{Solv}} \rightarrow [\text{K}(\text{COT})]_{\text{Solv}}$, we must accurately account for the entropy change associated with the process of ion pairing, for which the simple model used herein is not suited.²² For the special case of the disproportionation reaction, it is reasonable to expect the entropy for the two half-reactions $[\text{K}(\text{COT})] + \text{e}^- + \text{K}^+ \rightarrow [\text{K}_2(\text{COT})]$ and $[\text{K}(\text{COT})] \rightarrow \text{COT} + \text{e}^- + \text{K}^+$ to cancel, assuming the entropy changes of the first and second ion-pairing processes are similar. Second, computing the solvation energy of the K⁺ ion with a continuum model is not appropriate since a large reorganization energy of the highly solvated K⁺ ion to form the contact pair is expected.

(d) Summary. The DFT/COSMO model reproduces the experimentally established energy profiles of the 2e[−] redox processes correctly and suggests that the single 2e[−] behavior is favored only for the solvated ion pair model. The electrochemical behavior is primarily determined by electronic enthalpies, and the addition of the zero-point vibrational energy and entropy corrections does not change the relative energy differences significantly. For simplicity, the energy analysis presented below, which examines the features giving rise to the different energy profiles, will primarily use the uncorrected values.

Energy-Partitioning Scheme. As discussed above, an energetically favorable disproportionation reaction requires that the second reduction step ($\text{A}^{-1}/\text{A}^{-2}$) is more favorable than the first step (A^0/A^{-1}). If only vertical electron attachment energies in the gas phase are considered, the addition of the electron to a negatively charged particle should be more difficult than that to its neutral form, and the reaction enthalpy of a disproportionation reaction for bound systems in the gas phase will always be positive.²³ Solvation energy, which increases approximately as the square of the charge on the molecule,¹⁰ has a major impact on the energy profile for the redox reaction. In the Born model, the solvation energy of a dianion is approximately four times that of a monoanion. Therefore, stabilization due to solvation for a system where the most oxidized form is neutral favors the disproportionation reaction by increasing the energy difference of $\text{A}^{-1}/\text{A}^{-2}$ more than that of the A^0/A^{-1} pair. Although placing a molecule in solution dampens the impact of the added charge, the potential for the second reduction is typically more negative than the first, which can be characterized as classical redox behavior. When a nonclassical potential ordering is observed, a structural change associated with one of the two redox steps has been often cited as one of the main factors dictating multielectron redox behavior.⁷

Ion pairing introduces complications into this simple analysis, and several factors contribute to the energy changes on forming the ion pair. The cation is an electrophile, to which electron density is transferred from the anion, the nucleophile, and there

(19) (a) Reiss, H.; Heller, A. *J. Phys. Chem.* **1985**, *89*, 4207–4213. (b) Wheeler, R. A. *J. Am. Chem. Soc.* **1994**, *116*, 11048–11051. (c) Boesch, S. E.; Grafton, A. K.; Wheeler, R. A. *J. Phys. Chem.* **1996**, *100*, 10083–10087. (d) Mook, K. H.; Macgregor, S. A.; Heath, G. A.; Derrick, S.; Boere, R. T. *J. Chem. Soc., Dalton Trans.* **1996**, 2067–2076. (e) Macgregor, S. A.; Mook, K. H. *Inorg. Chem.* **1998**, *37*, 3284–3292. (f) DiLabio, G. A.; Pratt, D. A.; LoFaro, A. D.; Wright, J. S. *J. Phys. Chem. A* **1999**, *103*, 1653–1661. (g) Li, J.; Fisher, C. L.; Chen, J. L.; Bashford, D.; Noodleman, L. *Inorg. Chem.* **1996**, *35*, 4694–4702. (h) Konecny, R.; Li, J.; Fisher, C. L.; Dillet, B.; Bashford, D.; Noodleman, L. *Inorg. Chem.* **1999**, *38*, 940–950. (i) Li, J.; Nelson, M. R.; Peng, C. Y.; Bashford, D.; Noodleman, L. *J. Phys. Chem. A* **1998**, *102*, 6311–6324. (j) Li, J.; Fisher, C. L.; Konecny, R.; Bashford, D.; Noodleman, L. *Inorg. Chem.* **1999**, *38*, 929–939. (k) Mouesca, J.-M.; Chen, J. L.; Noodleman, L.; Bashford, D.; Case, D. A. *J. Am. Chem. Soc.* **1994**, *116*, 11898–11914. (l) Winget, P.; Weber, E. J.; Cramer, C. J.; Truhlar, D. G. *Phys. Chem. Chem. Phys.* **2000**, *2*, 1231–1239. (m) Kettle, L. J.; Bates, S. P.; Mount, A. R. *Phys. Chem. Chem. Phys.* **2000**, *2*, 195–201. (n) Reynolds, C. A. *Int. J. Quantum Chem.* **1995**, *56*, 677–687. (o) Raymond, K. S.; Grafton, A. K.; Wheeler, R. A. *J. Phys. Chem. B* **1997**, *101*, 623–631. (p) Baik, M.-H.; Ziegler, T.; Schauer, C. K. *J. Am. Chem. Soc.* **2000**, *122*, 9143–9154.

(20) The reports on electrochemical measurements commonly use SCE or Ag/AgCl as the reference electrodes. We have converted these values to SHE referenced potentials by adding 0.2412 V (SCE) or adding 0.197 V (Ag/AgCl) according to ref 23.

(21) Note that the two terms $\Delta\Delta E(\text{disp})$ and ΔE° (or $\Delta E_{1/2}$ if the experimental half-wave potentials are compared) both refer to the potential difference. The former is more natural from the computational standpoint, where the potential E° is computed as the energy difference of the redox pair, and the later is the more familiar term from the experimental viewpoint.

(22) This is the same dilemma one encounters, e.g., in pK_a calculations where the explicit solvent reorganization energy of the solvated proton has to be accounted for in a continuum solvation calculation. For typical approaches to deal with this problem, see for example: (a) Orlov, V. M.; Smirnov, A. N.; Varshavsky, Y. M. *Tetrahedron Lett.* **1976**, *48*, 4377–4378. (b) Lyne, P. D.; Karplus, M. *J. Am. Chem. Soc.* **2000**, *122*, 166–167. (c) Richardson, W. H.; Peng, C.; Bashford, D.; Noodleman, L.; Case, D. A. *Int. J. Quantum Chem.* **1997**, *61*, 207–217. (d) Li, J.; Fisher, C. L.; Konecny, R.; Bashford, D.; Noodleman, L. *Inorg. Chem.* **1999**, *38*, 929–939. (e) Chen, J. L.; Noodleman, L.; Case, D. A.; Bashford, D. *J. Phys. Chem.* **1994**, *98*, 11059–11068. (f) Baik, M.-H.; Silverman, J. S.; Yang, I. V.; Ropp, P. A.; Szalai, V. A.; Yang, W.; Thorp, H. H. *J. Phys. Chem. B* **2001**, *105*, 6437–6444.

(23) This phenomenon is known as the *convexity principle*, for which no formal proof exists. However, there is no known example of a system where this principle is violated for purely and intrinsically electronic reasons. See ref 9a, p 72.

is an attractive Coulombic interaction between the ions of opposite charge. The formation of an overall neutral system from two separated charged systems results in loss of solvation energy due to the loss of solute/solvent contact surface, as well as to the charge transfer between the ions, which leads to partial charge neutralization. To attain a better understanding of the redox behavior in these systems, it is desirable to partition the energy change upon reduction in a meaningful way to address which factors dictate the observed electrochemical behavior of a particular system.

Several energy-partitioning schemes have been proposed in the literature, of which two schemes, one developed by Ziegler and Rauk^{24a} and the other by Morokuma,^{24b} are most commonly used. Any energy-partitioning analysis is governed by the formal definition of the energy terms, which is not unambiguous, so the choice of the scheme should be guided by the chemical purpose of the analysis. This study focuses on changes in structure and charge distribution as a function of redox state. These two main features subject to electronically driven changes are of course coupled and a simple deconvolution is difficult. In electrochemical reaction schemes, the electrochemical and chemical reactions (e.g. EC or CE mechanism²⁵) are formally deconvoluted by square schemes that separate the chemical and electrochemical steps. This same principle has been applied to our theoretical results and *theoretical square schemes* have been constructed to decompose the reduction reaction into a “semi-adiabatic electron attachment energy” and a “structural relaxation energy”. The term semi-adiabatic refers to the fact that upon electron addition (or removal), electronic relaxation is allowed in a field of frozen nuclei. This is only a formal energy partitioning and does not reflect the real electron-transfer process.

An energy decomposition diagram for the gas-phase model is shown in Figure 3a. Construction of the upper left quadrant will be described. A single-point calculation is carried out using the optimized geometry of the neutral tub-COT with a total charge of -1 , and the energy difference between tub-COT and tub-(COT)⁻¹ is represented on the line connecting these two structures (Step Ia). Likewise, the energy of the lower left corner is arrived at by carrying out a single-point calculation on the planar optimized geometry of (COT)⁻¹, but with neutral charge; the energy difference between planar-COT and planar-(COT)⁻¹ is represented by Step Id. The vertical steps Ic and Ib represent the structural relaxation energy for conversion of tub-COT to planar-COT, and tub-(COT)⁻¹ to planar-(COT)⁻¹, respectively. The analogous procedure is repeated for completion of the remainder of the diagram. Energy partitioning diagrams have also been constructed for the solvated ions (Figure 3b) and the solvated ion pairs (Figure 3c). To keep all three diagrams analogous, for the ion-pair case, the addition of an electron and a potassium cation have not been divided in two steps, but this will be done separately.²⁶ On the basis of this analysis, the energy change upon reduction can be formally partitioned into

four parts: (i) the semi-adiabatic electron attachment energy; (ii) structural relaxation, which occurs to relax the electronic tension introduced by the additional charge; (iii) the Coulombic solvation energy; and (iv) ion-pair formation. These four factors are discussed below. The energies for the theoretical square schemes from both program packages, DMol and ADF, are in excellent agreement and lead to the same conclusions. The numerical results presented below are primarily DMol results and are not ZPE/entropy corrected.

(a) Semi-Adiabatic Electron Attachment Energies, Solvation, and Structural Relaxation. For the COT molecule, in the absence of structural relaxation, the qualitative expectation that sequential electron additions are less energetically favored is demonstrated in the gas-phase model and the solvated ion models. The semi-adiabatic electron attachment energies, along each row in the square scheme diagrams (Figure 3a,b), are successively more positive for each structure. In the gas phase, the two-electron attachment energies are 0.3 eV/5.8 eV, -1.2 eV/4.1 eV, and -1.2 eV/3.8 eV for the tub-shaped D_{4h} , and D_{8h} structures, respectively. The addition of the second electron is therefore a highly unfavorable process in the gas phase, and the second electron is unbound regardless of the final geometry considered. If solvation is included, all electron-attachment processes are downhill, and the relative magnitude of the two reduction potentials becomes much more reasonable. The three possible structures give electron-attachment energies of -2.1 eV/ -1.0 eV, -3.6 eV/ -2.6 eV, and -3.6 eV/ -2.8 eV for the tub-shaped D_{4h} and D_{8h} structures, respectively, displaying classical behavior in all cases.

The major structural change that takes place from reduction of tub-COT to planar-(COT)⁻¹ has a substantial influence on the reduction potential of (COT)⁻¹, and the semi-adiabatic electron attachment energy for planar (COT)⁻¹ (Figure 3b, Step IVa: -60 kcal/mol) is 12 kcal/mol more negative than that for COT (Figure 3b, Step IIIa: -48 kcal/mol), despite the fact that planar-(COT)⁻¹ bears a negative charge. The impact of the structural change on the redox potential is the most important factor in dictating the overall energy profile of the disproportionation reaction. As described above, COT displays a large structural distortion to a planar structure in the first step, and our analysis scheme assigns a structural relaxation energy of -24 kcal/mol for the first reduction step (Figure 3a, Step Ib). By comparison, the energy associated with transformation of the D_{4h} structure to the D_{8h} structure of -3 kcal/mol in the second step (Step IIb) is insignificant. Notably, the energies assigned to the structural relaxation are essentially identical in the gas-phase, solvated ion, and solvated ion-pair models (Steps Ib/IIIb/Vb and IIb/IVb/VIb). Step IIIc gives the ring-flattening energy of the neutral COT molecule in solution, and this quantity is experimentally accessible through spectroscopic methods. Strauss et al.^{6g} have estimated this energy to be 13.7 kcal/mol at 10 °C, which is in good agreement with the computed energy of 10 kcal/mol assigned for this process.

(b) Impact of Ion Pairing on the Energy Profile. The first step in understanding the features leading to the distortion of the energy profile if ion-pair formation is allowed is to identify the relative magnitude of the energy changes that the ion-pairing process has on the first- and second-electron additions. Table 4 compares the energy balances of the two half reactions COT \rightarrow (COT)⁻¹ and (COT)⁻¹ \rightarrow (COT)⁻² with and without

(24) (a) Ziegler, T.; Rauk, A. *Theor. Chim. Acta* **1977**, *46*, 1–10. (b) Kitaura, K.; Morokuma, K. *Int. J. Quantum Chem.* **1976**, *10*, 325–340.

(25) For an overview of these basic classes of coupled reactions, see for example: Bard, A. J.; Faulkner, L. R. *Electrochemical Methods—Fundamentals and Applications*; John Wiley & Sons: New York, 1980.

(26) The K–COT distances involving nonstandard COT geometries at a given charge, that is, e.g. tub-shaped COT with a charge of -1 , have been fully optimized with a constrained COT geometry.

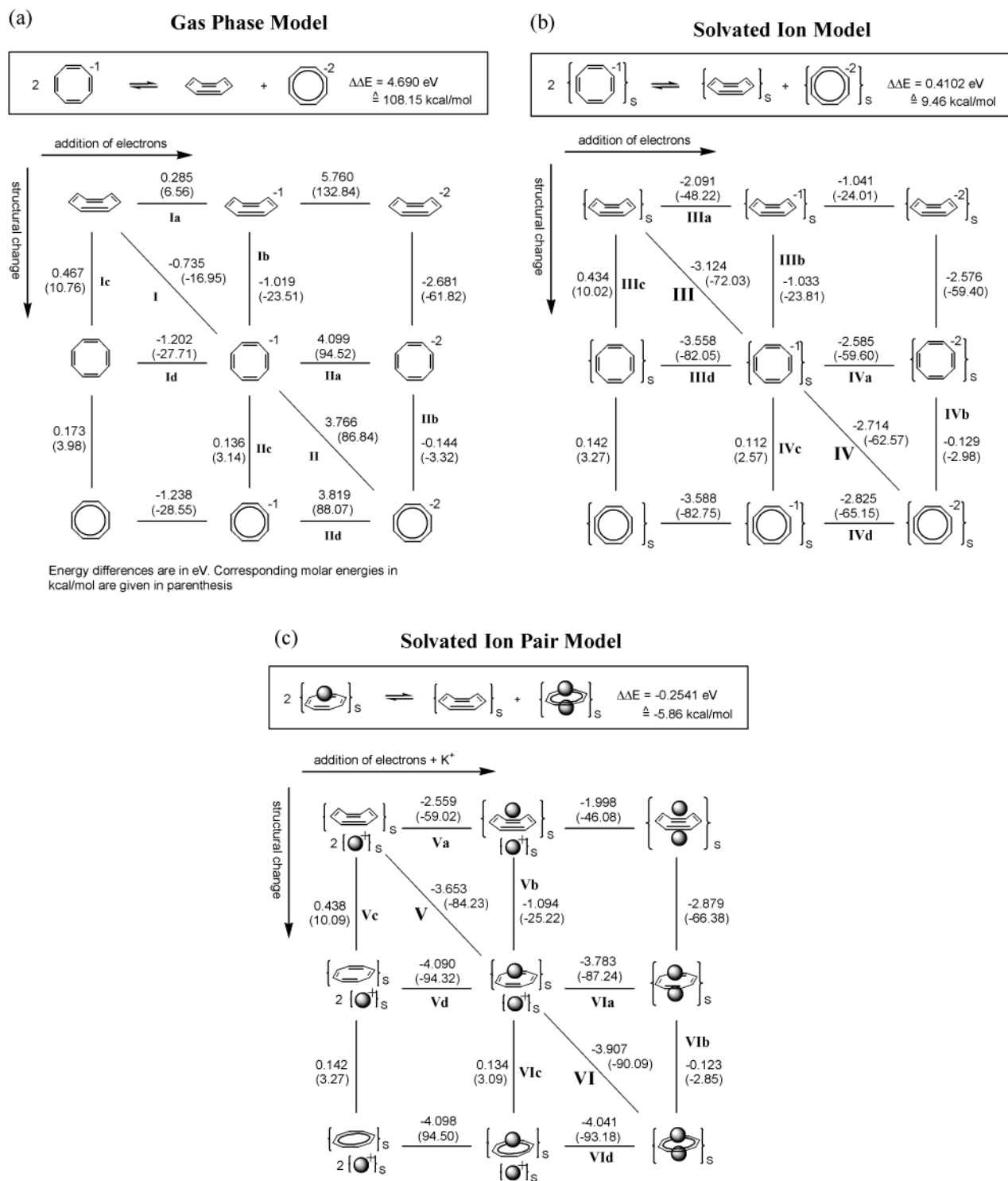


Figure 3. Energy partition scheme of the two-electron reduction of cyclooctatetraene (DMol results). Energies are given in eV and the corresponding molar energies in kcal mol⁻¹ are given in parentheses.

Table 4. Energy Balance for the Half Reaction of the COT Reduction (in kcal/mol) in Ammonia Solvent (DMol energies)

	solv. ion	solv. ion pair	difference
(0) → (-1)	-71.0	-84.2	-13.3
(-1) → (-2)	-59.8	-90.1	-30.3
$\Delta\Delta E(\text{disp})$	11.2	-5.9	

ion-pair formation. In the square scheme, this corresponds to taking the difference between energies for steps V and III and

steps VI and IV, for the first and second ion reduction steps, respectively. The ion-pair formation gives an additional stabilization of -13 kcal/mol for the addition of the first electron, whereas the formation of the ion-pair [K₂(COT)] from [K(COT)]⁻¹ and a free K⁺ ion including the reduction process gives a stabilization energy of -30 kcal/mol, which is large enough to shift the disproportionation equilibrium (eq 2) to the right side. The disproportionation enthalpy changes by -15 kcal/

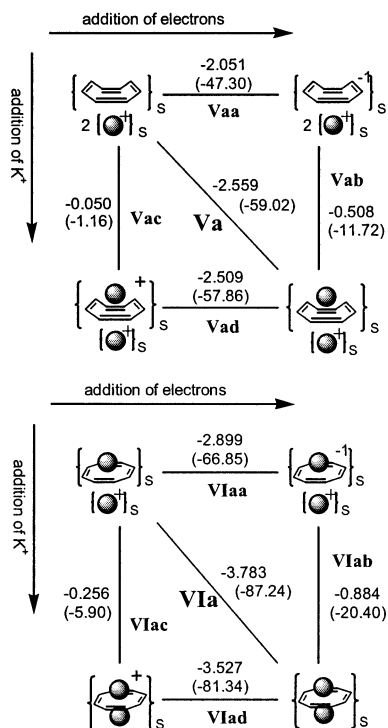


Figure 4. Energy decomposition of the ion pairing steps for cyclooctatetraene (DMol results).

mol from +9 kcal/mol for the solvated ion model to -6 kcal/mol (Figure 3), and becomes a thermodynamically downhill process.

As discussed above, the energy change arising from the structural relaxation (Step IIIb/Vb and Step IVb/VIb) stays nearly constant for the solvated ion and ion-pair systems, therefore the important changes in the energy profile as a result of ion pairing lie in a comparison of Steps IIIa/Va and Steps IVa/VIa. For the ion-pair systems, Steps Va and VIa can be further partitioned into the semi-adiabatic electron-attachment energy and ion-pair formation components as shown in Figure 4. The first semi-adiabatic electron-attachment energy in the ion-pair system (Figure 4, Step Vaa) is equal to that of the solvated ion model in ammonia solvent. The second semi-adiabatic electron-attachment energy in the solvated ion model can be compared to that of the ion-pair model by comparing Steps IVa and VIaa in the same solvent. Step IVa gives an energy difference of -57 kcal/mol in ammonia, whereas an energy difference of -67 kcal/mol is calculated for the analogous process for the neutral [K(COT)] ion pair (Step VIaa). As expected, the semi-adiabatic electron-attachment energy for the [K(COT)] ion pair is favored over that of the (COT)⁻¹ ion (by -10 kcal/mol). The partial delocalization of the added charge onto the potassium ion reduces the repulsive interaction for the second electron.

The LUMO of [K(COT)] shown in Figure 5 is closely related to the LUMO of (COT)⁻¹. Since the LUMO is the electron-accepting orbital, a correlation of the LUMO energy with semi-adiabatic electron-attachment energy is expected. Table 5 compares the LUMO-based estimates of the electron-attachment energy with those presented in Figure 4. The LUMO-based estimates are -2.33 eV (COT) and -3.46 eV ([K(COT)]) for the first and second reductions, respectively, demonstrating that [K(COT)] is a better electrophile than (COT)⁻¹. The semi-

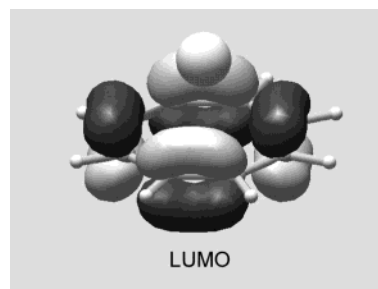


Figure 5. LUMO of [K(COT)].

Table 5. Electron Attachment Energies of COT and [K(COT)] (in eV) Computed with the LUMO Energy (E^{LUMO}) and the Total Energy Difference of the Nonrelaxed Structures ($E^{\Delta\text{Tot}E}$)

	COT	[K(COT)]	difference
E^{LUMO}	-2.33 ^a	-3.46 ^b	-1.13
$E^{\Delta\text{Tot}E}$	-2.05 ^c	-2.90 ^d	-0.85

^a LUMO energy of COT⁰ in ammonia (see Table 2). ^b β -LUMO energy of [K(COT)]. Note that [K(COT)] is an open-shell system, thus the true LUMO is the β -spin-orbital corresponding to the α -HOMO. In Table 1 only the α -spin-orbitals are given. The β -LUMO energy is -3.462 eV, which is 0.06 eV higher than the α -HOMO in our unrestricted spin calculation. ^c Step Vaa in Figure 4. ^d Step VIaa in Figure 4.

adiabatic reduction potential, computed as the total energy differences of the unrelaxed geometries, gives values of -2.05 and -2.90 eV for Step Vaa and Step VIaa, respectively (Figure 4). The differences in the values calculated by these two different methods are significant, 0.28 and 0.56 eV respectively for the first- and second-reduction steps. However, for both methods, the second reduction is energetically more downhill than the first, correctly predicting a 2e⁻ redox behavior.

After the electron-addition steps, the ion-pairing events take place (Figure 4, Steps Vab and VIab) to form [K(COT)] and [K₂(COT)], giving rise to stabilizations of -12 and -20 kcal/mol, respectively. For the first ion-pair formation step, (COT)⁻¹ + K⁺ → [K(COT)], the partial charge at carbon based on a Hirshfeld charge analysis scheme (Table 6) changes from -0.13 in the (COT)⁻¹ ion by +0.03 upon ion-pair formation to -0.10 in [K(COT)]. For the second step, [K(COT)]⁻¹ + K⁺ → [K₂(COT)], the partial charge of -0.18 in [K(COT)]⁻¹ changes by +0.03 to -0.15 in [K₂(COT)]. The charge of the potassium ions remain approximately constant at +0.6 (+0.64 in [K(COT)], and +0.59 in [K₂(COT)]). The higher ion-pairing energy for the addition of the second potassium ion can be rationalized to be a consequence of the higher negative charge at the COT fragment, which gives rise to a larger Coulombic interaction.

Both rationalizations of the energy shifts to the electron-attachment energies given above are intuitive. Adding a counterion to an anion will always result in a more negative electron-attachment energy in comparison to the parent anion, and the addition of a second electron to a monopotassium ion pair will increase the partial charge on the anionic fragment, giving rise to a larger electrostatic interaction with the second cation. Thus, the question arises naturally whether or not these straightforward energy decomposition results are sufficient to explain the unusual redox behavior of COT. To contrast the specific features of the COT energy profiles described above, we have applied the same theoretical protocol to nitrobenzene (NB), a molecule that displays two well-separated 1e⁻ redox potentials in both DMF/NMe₄Br and ammonia/KI.¹¹

Table 6. Hirshfeld Charges of COT as a Function of Oxidation State, Geometry, and Ion Pairing

	C	H	K
equilibrium geometries			
tub-(COT)	-0.046	+0.046	
planar-(COT) ⁻¹	-0.128	+0.003	
planar-(COT) ⁻²	-0.209	-0.041	
planar-[K(COT)]	-0.100	+0.020	+0.640
planar-[K(COT)] ⁻¹	-0.176	-0.024	+0.602
planar-[K ₂ (COT)]	-0.146	+0.002	+0.591
nonequilibrium geometries			
tub-(COT) ⁻¹	-0.125	0.000	
tub-[K(COT)]	-0.105/-0.104	+0.011/+0.019	+0.717
charge differences			
planar-(COT) ⁻¹ - tub-(COT)	-0.082	-0.036	
planar-(COT) ⁻² - planar-(COT) ⁻¹	-0.081	-0.044	
planar-[K(COT)] - planar-(COT) ⁻¹ + K ⁺	+0.028	+0.017	-0.360
planar-[K ₂ (COT)] - planar-[K(COT)] ⁻¹ + K ⁺	+0.030	+0.026	-0.420

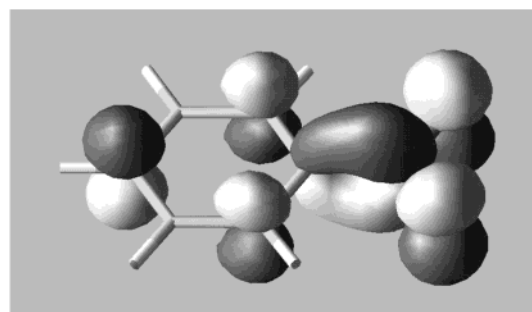
Table 7. Gas-Phase and COSMO Structures of Nitrobenzene with Selected Bond Lengths (in Å)

	NB	(NB) ⁻¹ -NB	(NB) ⁻¹	(NB) ⁻² -(NB) ⁻¹	(NB) ⁻²
gas phase					
N2-O13/N2-O14	1.246	0.058	1.304	0.051	1.355
C1-N2	1.493	-0.086	1.407	-0.056	1.351
C1-C3/C1-C11	1.400	0.029	1.429	0.041	1.470
C3-C5/C9-C11	1.398	-0.004	1.394	-0.006	1.388
C5-C7/C7-C9	1.403	0.012	1.415	0.024	1.439
COSMO					
N2-O13/N2-O14	1.262	0.066	1.328	0.056	1.384
C1-N2	1.468	-0.065	1.403	-0.059	1.344
C1-C3/C1-C11	1.405	0.020	1.425	0.035	1.460
C3-C5/C9-C11	1.400	-0.001	1.399	-0.006	1.393
C5-C7/C7-C9	1.407	0.006	1.413	0.012	1.425

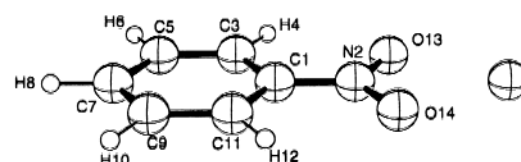
Structural Parameters and Energy Profiles for Nitrobenzene (NB) Reduction. NB undergoes a much simpler structural change upon reduction. Table 7 shows the relevant nuclear distances of the different optimized redox states of the molecule. The LUMO of the neutral species is mainly localized at the NO₂ fragment and is a π -type orbital that is N-O antibonding and N-C bonding (Figure 6a). The occupation of this orbital is therefore expected to elongate the N-O bonds and shorten the N-C bond. In gas phase the N-O distances increase by 0.05 Å for each addition of an electron, whereas the N-C distance decreases by 0.09 and 0.06 Å, respectively.

For the structure of the ion pair, we have explored a series of possible geometries. Most likely, the K⁺ ion will be attracted to the NO₂ fragment, but π -interactions with the arene ring were also considered. The most stable structures for the mono- and dipotassium ion pairs are shown in Figure 6, parts b and c, respectively. Table 8 gives the relevant bond distances of the optimized structures and Table 9 summarizes the energies of the solvated ion and solvated ion-pair models. In [K(NB)], the K⁺ ion is centered between the oxygen atoms and is coplanar with the ring (K-O = 2.694 Å). In [K₂(NB)] two K⁺ ions are both coordinated to the nitro group, where one K⁺ ion lies above and the other lies below the molecular plane; the K-O distance decreases slightly to 2.664 Å. Since the K⁺ ion occupies a

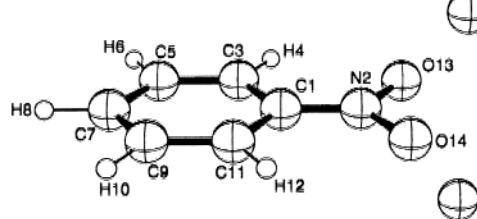
(a)



(b)



(c)

**Figure 6.** (a) HOMO of (NB)⁻¹. (b) Optimized structure of [K(NB)]. (c) Optimized structure of [K₂(NB)].**Table 8.** Selected Bond Lengths (in Å) of the NB Ion Pair^a

	[K(NB)]	[K ₂ (NB)]
N2-O13/N2-O14	1.335	1.405
C1-N2	1.404	1.351
C1-C3/C1-C11	1.422	1.447
C3-C5/C9-C11	1.400	1.397
C5-C7/C7-C9	1.411	1.418
O13-K	2.694	2.664

^a Labels are assigned in Figure 6.

different coordination site in these two structures, a direct comparison of the K-O distance is not appropriate.

The energy profiles of the electron-addition process for the gas phase, solvated ion, and solvated ion-pair models for

Table 9. Energies of Optimized Nitrobenzene Structures in Solution with and without Ion Pairing

	NB	(NB) ⁻¹	(NB) ⁻²	[K(NB)]	[K ₂ (NB)]
DMol3					
total <i>E</i> ^a	-436.805	-436.932	-437.011	-1036.824	-1636.810
LUMO ^b	-3.77	-0.87	0.02	-1.05	-0.41
HOMO ^c	-6.71	-2.83	-1.63	-3.29	-2.44
<i>E</i> (solv) ^d	-8.29	-62.68	-206.76	-24.39	-39.55
ADF					
binding <i>E</i> ^e	-86.95	-90.48	-92.87	-89.13	-90.29
LUMO ^b	-3.78	-1.10	-0.33	-1.11	-1.18
HOMO ^c	-6.89	-3.62	-2.34	-3.42	-2.57
<i>E</i> (solv) ^d	-9.21	-76.24	-240.71	-18.96	-32.48

^a Total SCF energy in au. ^b Lowest Unoccupied molecular orbital energy in eV; as a result of the unrestricted formalism the LUMO of the doublet (NB)⁻¹ and [K(NB)] are technically the β -spin-orbitals of the highest occupied orbitals. To allow comparison with the LUMO energies of (NB)⁻² and [K₂(NB)] the energies of the empty orbital with the same spin are given. ^c Highest Occupied molecular orbital energy in eV. ^d Electrostatic solvation energy in kcal/mol. ^e Binding energy in eV: ADF computes binding energies rather the absolute SCF energies, which are defined as the total molecular energy – the sum of the atomic fragment energies.

nitrobenzene reduction are shown in Figure 7. Table 10 summarizes the computed and experimental redox potentials, and the total reaction energy balance of the disproportionation reactions, $\Delta\Delta E(\text{disp})$. Unlike the COT molecule, nitrobenzene displays energy profiles in which the disproportionation reaction is uphill for all three models. The total energy balance, $\Delta\Delta E(\text{disp})$, is +1.28 eV (DMol)/+1.15 eV (ADF) if only solvation is considered. Ion pairing gives rise to a shift of the total energy difference by 0.34 eV (DMol)/0.15 eV (ADF) to a

$\Delta\Delta E(\text{disp})$ value of +0.94 eV (DMol)/+1.00 eV (ADF). The negative shift of $\Delta\Delta E(\text{disp})$ by 0.34 eV as a result of ion pairing for NB is smaller than the energy difference that accompanied the ion-pairing event in COT of 0.7 eV (Table 3).

The electrochemistry of nitrobenzene has been examined in DMF/Me₄N⁺Br⁻ solvent and in liquid ammonia/KI.^{11a,d} In DMF with the noncoordinating electrolyte Me₄N⁺Br⁻ (using CV), two reduction waves are observed at -0.85 and -1.91 V vs SHE.^{11d} These potentials are in reasonable agreement with the calculated potentials for the solvated ion model of -0.90 and -2.16 V vs SHE in DMF solvent, respectively. Our solvated ion model calculation overestimates the potential separation by 200 mV ($\Delta E^\circ(\text{calc}) = 1.26$ V vs $\Delta E^\circ(\text{exp}) = 1.06$ V). In ammonia/KI, two reversible reductions are observed separated by 0.82 V^{11a} at -0.22 and -1.04 V vs SHE. This $\Delta\Delta E(\text{disp})$ value²⁶ is in fair agreement with the calculated value of 1.14 eV (DMol) including ZPE/entropy corrections for the solvated ion-pair model (Table S10, Supporting Information).

Semi-Adiabatic Electron Attachment Energies, Solvation, and Structural Relaxation. In the following we will discuss the energy shifts of the NB system and compare them to COT using the energy-partitioning diagram shown in Figure 8. Both neutral and monoanionic nitrobenzene species have larger semi-adiabatic electron attachment energies than the neutral and monoanionic cyclooctatetraene, respectively, as indicated by the energy differences of the respective species. Whereas the semi-adiabatic electron-attachment energy for the neutral COT molecule is energetically uphill in gas phase (Figure 3a, Step

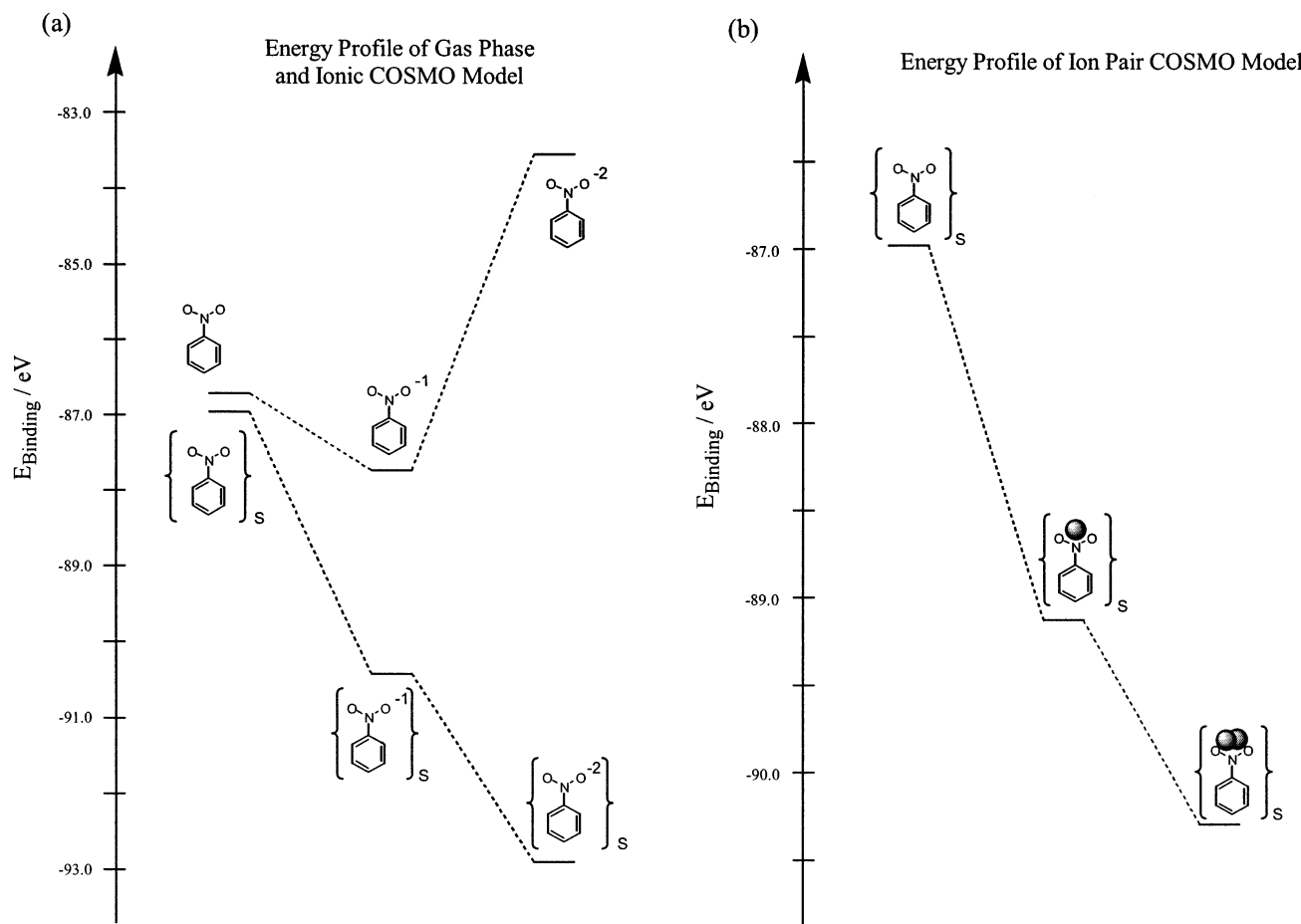
**Figure 7.** Total binding energies (ADF results) of the three redox states of nitrobenzene for gas phase, solvated ion, and solvated ion-pair models.

Table 10. Calculated Reduction Potentials Based on Electronic Enthalpy Only ($E^\circ(\Delta H)$) and the Gibbs Free Energy ($E^\circ(\Delta G)$) for NB^a and Experimental Reduction Potentials (in V) vs SHE

(a) Calculated Reduction Potentials						
	(0) → (-1)		(-1) → (-2)		$E_1^\circ - E_2^\circ = \Delta\Delta E(\text{disp})$	
	$\Delta E_1/E_1^\circ (\Delta H)$	$\Delta E_1/E_1^\circ (\Delta G)$	$\Delta E_2/E_2^\circ (\Delta H)$	$\Delta E_2/E_2^\circ (\Delta G)$	ΔH	ΔG
DMol3						
solv. ion (DMF)	-3.45/-0.98	-3.53/-0.90	-2.17/-2.26	-2.27/-2.16	1.28	1.26
solv. ion pair (NH ₃)	-4.18	-4.43	-3.24	-3.29	0.94	1.14
ADF						
solv. ion (DMF)	-3.53/-0.90	-3.61/-0.82	-2.39/-2.04	-2.48/-1.95	1.15	1.13
solv. ion pair (NH ₃)	-2.15	-2.41	-1.16	-1.21	1.00	1.19
(b) Experimental Reduction Potentials						
experimental	E_1° : (0) → (-1)	E_2° : (-1) → (2)	$E_1^\circ - E_2^\circ$			
solv. ion (DMF) ^b	-0.85	-1.91	1.06			
solv. ion pair (NH ₃) ^c	-0.22	-1.04	0.82			

^a In DMol3, we have added the SCF energy of the solvated K(+) ion on the reactant side for the reaction $\text{NB}^0 + \text{K}^+ + \text{e}^- \rightarrow [\text{K}(\text{NB})]$ and $[\text{K}(\text{NB})] + \text{K}^+ + \text{e}^- \rightarrow [\text{K}_2\text{NB}]$. In ADF, this correction is not necessary, since the binding energies are computed and the energies are all normalized to the sum of the fragment energies. Therefore ADF results are referenced to the reaction $\text{NB}^0 + \text{K}^0 \rightarrow [\text{K}(\text{NB})]$ and $[\text{K}(\text{NB})] + \text{K}^0 \rightarrow [\text{K}_2(\text{NB})]$. ^b Reference 11d. ^c Reference 11a.

Ia) and becomes a downhill process due to structural relaxation, NB displays an energetically favorable electron addition in gas phase without including the structural relaxation energy (Figure 8a, Step Ia). The semi-adiabatic reduction potential of NB is -17 kcal/mol, which increases to -73 kcal/mol if solvation energies are included. The addition of the structural relaxation term yields a total energy difference of -80 kcal/mol (Figure 8b, Step III) for the first addition of the electron in the solvated ion model. The second adiabatic electron-attachment energy (Figure 8b, Step IV) is -50 kcal/mol, so the total energy balance for the disproportionation reaction is roughly 30 kcal/mol in the solvated ion model.

As discussed above, for COT the second semi-adiabatic electron attachment energy (Figure 3, Step IVa) releases more energy than the first (Figure 3b, Step IIIa) in the solvated ion model. NB displays classical behavior, and the first step releases -73 kcal/mol (Figure 8b, Step IIIa), while the second releases -45 kcal/mol (Figure 8b, Step IVa). The minor structural relaxation of the $(\text{NB})^{-1}$ ion (see below) clearly does not have a great impact on the reduction potential of the relaxed species.

The asymmetric structural change that caused a significantly larger stabilization of the $(\text{COT})^{-1}$ molecule in comparison to $(\text{COT})^{-2}$ is not observed for NB. Overall the structural relaxation energies for NB are relatively small and of the same magnitude (5–6 kcal/mol) for each step in the overall 2e^- reduction process. It is noteworthy that the energy to adopt the equilibrium geometry for the electron-addition product prior to electron addition (Steps Ic, IIc, IIIc, and IVc) is nearly equal in magnitude and opposite in sign to the structural relaxation energy after electron addition (Steps Ib, IIb, Vb, and VIb). The first electron-addition step for COT has very different values for the two structural distortion energies, presumably because of the resonance stabilization possible in the planar structure.

Ion Pairing. The energy balances of the half reactions for the solvated ion and solvated ion-pair models (Figure 8, Step V–Step III and Step VI–Step IV) for NB are summarized in Table 11. The ion pairing of K^+ with $(\text{NB})^{-1}$ gives an additional stabilization of -18 kcal/mol for the first reduction step, while the addition of the second K^+ ion to $[\text{K}(\text{NB})]^{-1}$ results in an additional stabilization of -27 kcal/mol for the second reduction

step. For COT these energies were -13 and -30 kcal/mol, respectively (Table 4). The negative shift of $\Delta\Delta E(\text{disp})$ upon ion-pair formation is 7 kcal/mol larger for COT than for NB.

As for COT, the energies of Steps Va and VIa are further partitioned into the semi-adiabatic electron-attachment energy and ion-pair formation components as shown in Figure 9. By comparing the energies for Steps VIa and IVa, it can be assessed that coordination of the K^+ ion to the $(\text{NB})^{-1}$ ion gives rise to a shift in the semi-adiabatic electron-attachment energy of -5 kcal/mol (from -45 kcal/mol to -50 kcal/mol).

The semi-adiabatic electron attachment energies are compared in Table 12 with the estimates based on the LUMO energies of NB and $[\text{K}(\text{NB})]$. As for COT, the LUMO energy is consistently shifted by 0.5 eV from the respective semi-adiabatic electron-attachment energy. The semi-adiabatic electron-attachment energy decreases by 1.02 eV for $[\text{K}(\text{NB})]$ in comparison to NB, and the corresponding value calculated based on the LUMO energies is 1.17 eV. For NB as well, the qualitative frontier orbital tool correctly predicts the relative values of the two 1e^- reduction potentials.

The ion-pairing events that take place after the electron-addition steps (Steps Vab and VIab) to form $[\text{K}(\text{NB})]$ and $[\text{K}_2(\text{NB})]$, respectively, give rise to stabilizations of -17 and -19 kcal/mol, respectively, to be compared to the corresponding values of -12 and -20 kcal/mol for COT. A majority of the greater shift observed for the first reduction potential as a result of ion pairing for NB in comparison to COT can be attributed to the greater ion-pairing energy in Step Vab for NB.

The distribution of the added charge clearly plays a role in determining the ion-pairing energies. Hirshfeld charges for different nitrobenzene anions and ion pairs are given in Table 13. In nitrobenzene, the first addition of an electron to form $(\text{NB})^{-1}$ changes the charge of the nitro group by -0.55 and -0.45 of the excess charge is dissipated on the phenyl group. The charge on the oxygen atoms in the nitro group changes from -0.21 to -0.42 upon reduction. The phenyl group plays a slightly larger role in the dissipation of the second electron, and -0.58 of the second charge is apportioned to the phenyl group, with the remainder of -0.42 to the NO_2 group. In $(\text{NB})^{-2}$, the charge on the oxygen atoms of the nitro group is -0.58. In the first ion-pair formation step, $\text{K}^+ + (\text{NB})^{-1} \rightarrow$

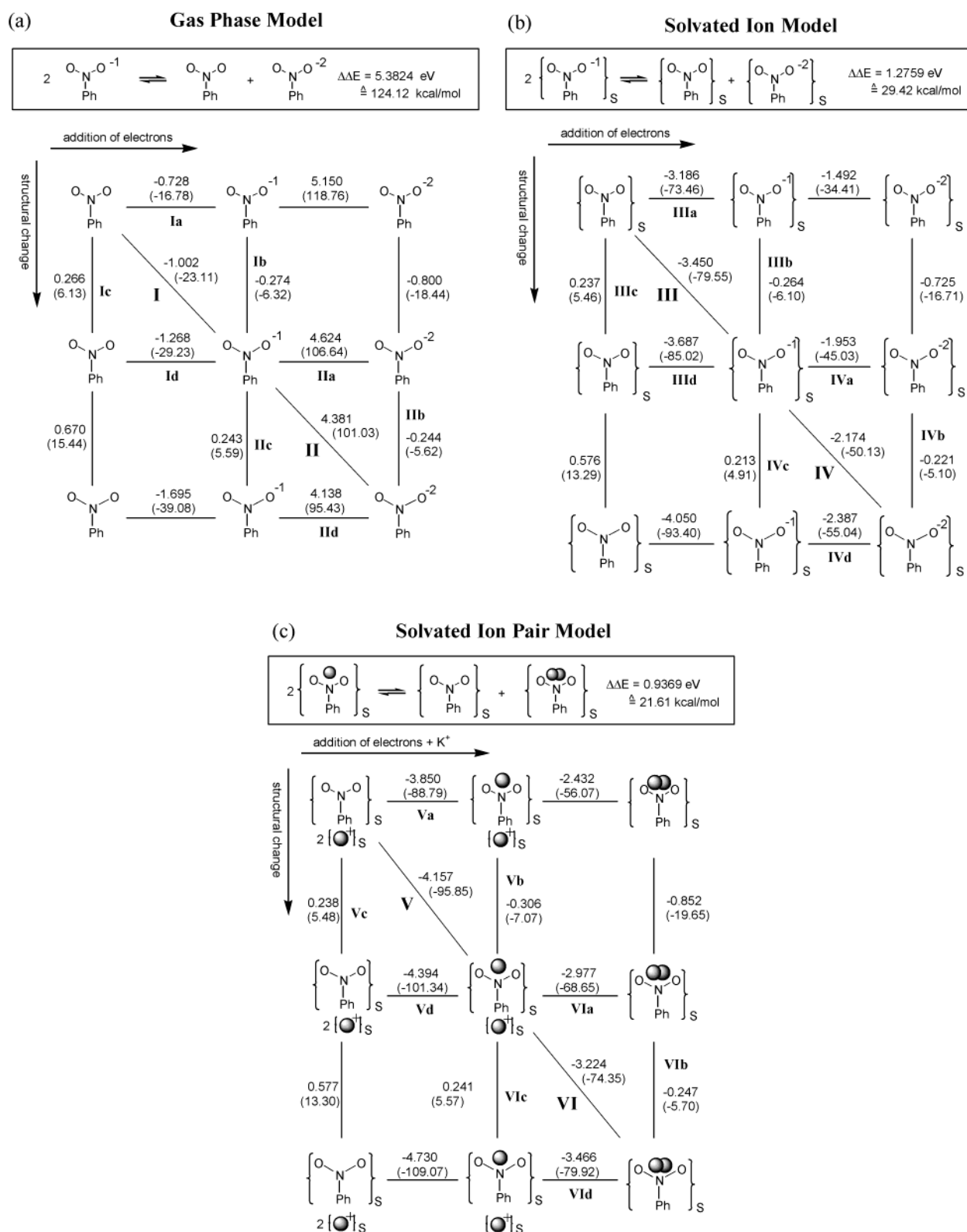


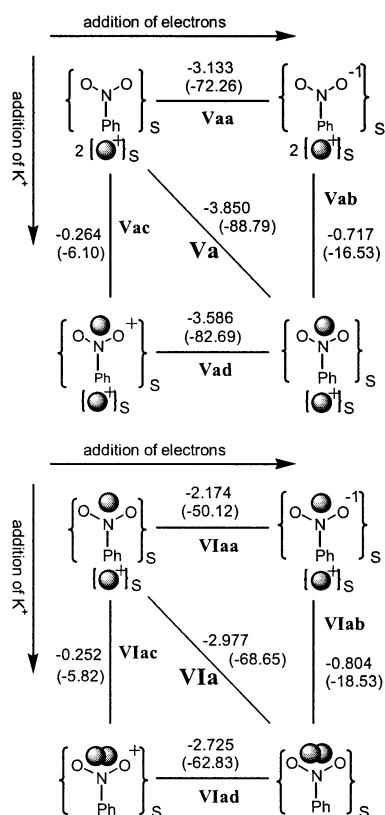
Figure 8. Energy partition scheme of the two-electron reduction of nitrobenzene (DMol results). Energies are given in eV and the corresponding molar energies in kcal mol⁻¹ are given in parentheses.

[K(NB)], a charge of -0.28 is transferred from the (NB)⁻¹ fragment to the initially free K⁺ ion upon ion pair formation, leaving a charge of $+0.72$; 72% of the transferred charge (0.20) comes from the NO₂ group, and the resulting charge on the oxygen atoms increases by $+0.09$ in [K(NB)] to -0.33 .

Analogously, in the second ion pair formation step, K⁺ + [K(NB)]⁻¹ → [K₂(NB)], a charge of -0.34 is removed from the [K(NB)]⁻¹ fragment, leaving a formal charge of $+0.66$ on the potassium ions in [K₂(NB)]. In this case, only 34% of the transferred charge (0.12) comes from the NO₂ group, and the

Table 11. Energy Balance for the Half Reactions of the NB Reduction (in kcal/mol)

	solv. ion (in DMF)	solv. ion pair (in NH ₃)	difference
(0) → (-1)	-79.56	-96.3	-17.8
(-1) → (-2)	-50.13	-74.7	-27.4
ΔΔ <i>E</i> (disp)	29.42	21.6	

**Figure 9.** Energy decomposition of the ion pairing steps for nitrobenzene (DMol results).**Table 12.** Electron Attachment Energies of NB and [K(NB)] (in eV) Computed Using the LUMO Energy (E^{LUMO}) and the Total Energy Difference of the Nonrelaxed Structures ($E^{\Delta\text{Tot}E}$)

	NB	[K(NB)]	difference
E^{LUMO}	-3.77	-2.60	1.17
$E^{\Delta\text{Tot}E}$	-3.19	-2.17	1.02

Table 13. Hirshfeld Charges for Different Species of Nitrobenzene

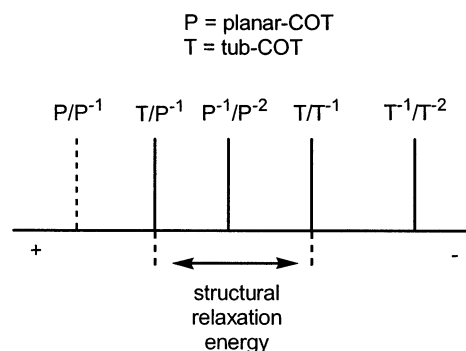
	C ₆ H ₅	N	O	K
NB	+0.232	+0.194	-0.213	
(NB) ⁻¹	-0.218	+0.056	-0.419	
(NB) ⁻²	-0.796	-0.039	-0.582	
[K(NB)]	-0.145	+0.089	-0.332	+0.721
[K(NB)] ⁻¹	-0.754	+0.001	-0.456	+0.667
[K ₂ (NB)]	-0.529	+0.010	-0.403	+0.663
(NB) ⁻¹ - NB	-0.449	-0.138	-0.207	
(NB) ⁻² - (NB) ⁻¹	-0.579	-0.096	-0.163	
[K(NB)] - (NB) ⁻¹ + K ⁺	+0.077	+0.032	+0.085	-0.279
[K ₂ (NB)] - [K(NB)] ⁻¹ + K ⁺	+0.225	+0.009	+0.053	-0.341

charge on the oxygen atoms increased by +0.06 in [K₂(NB)] from -0.46 to -0.40.

The Hirshfeld charge analyses (Tables 6 and 13) combined with the geometries of the ion pairs (Table 2 and Figure 6b) reveal that the ion-pair geometry of [K(COT)] allows full contact of the negative charge, which is delocalized over the carbon

Table 14. Total Energies and Ion Pairing Enthalpies (in hartrees; kcal/mol in parentheses) in Ammonia Solution

	A = COT	A = NB
K ⁺	-599.8669	-599.8669
A ⁻	-309.6556	-436.9295
[KA]	-909.5447	-1036.8241
[KA] ¹⁻	-909.6502	-1036.9040
[K ₂ A]	-1509.5541	-1636.8095
K ⁺ + A ⁻ → [KA]	-0.0212 (-13.3)	-0.0278 (-17.4)
K ⁺ + [KA] ¹⁻ → [K ₂ A]	-0.0370 (-23.2)	-0.0386 (-24.3)

**Figure 10.** A graph of the relative redox potentials for COT as a function of structure and redox state.

atoms, with the potassium ion. In [K(NB)], however, only that portion of the negative charge residing at the NO₂ fragment is close enough to potassium to interact strongly. The phenyl group in NB reduces the electrostatic interaction by partial removal of the excess charge from the center of direct interaction, where in COT there is no remote functional group to reduce the charge at the dianion.

The reaction enthalpy of the ion-pairing reaction can be calculated directly by combining fully relaxed anions with the cation to give a fully relaxed ion pair. The results of such a calculation for COT and NB are given in Table 14. In all cases, formation of the ion pair is thermodynamically downhill. The first ion-pair formation reaction for (COT)⁻¹ yields -13 kcal/mol and the second for [K(COT)]⁻¹ yields -23 kcal/mol. For NB the corresponding energies are -17 and -24 kcal/mol, respectively. By this equilibrium method, the separate factoring of the structural relaxation component to the ion pairing accessible in the square scheme analysis is not possible.

Summary and Implications

We have investigated the disproportionation energy profiles for cyclooctatetraene and nitrobenzene. The former displays a single 2e⁻ reduction process if ion pairing in solution is allowed, whereas nitrobenzene shows two distinct redox potentials regardless of the environmental conditions. Our theoretical model, which considers the relative stabilities of the reduction products, correctly distinguishes the nonclassical single 2e⁻ systems from molecules that exhibit two well-separated 1e⁻ potentials, and gives an intuitive explanation for the experimentally observed redox behavior.

The nonclassical redox behavior of COT is dictated by the structural change from the tub-shaped antiaromatic system to a planar pseudo-aromatic system in the first electron-addition step. The relationship between structure and redox potentials for COT is displayed graphically in Figure 10. Both the planar- and tub-COT structures display classical redox behavior, in which the

second semi-adiabatic reduction potential is more negative than the first. For a molecule where a major structural change accompanies the first reduction step like COT, the relative positioning of the redox potentials for the original structure T (=tub-COT) and the rearranged structure P (=planar-COT) is a key factor. The overall voltammetric behavior is dictated by the ordering of the T/P^{-1} and the P^{-1}/P^{-2} potentials. The structural relaxation energy in the first step determines how far positive the T/P^{-1} potential is shifted with respect to the T/T^{-1} potential, and therefore its positioning with respect to the P^{-1}/P^{-2} potential. The case of a molecule in which the major structural rearrangement accompanies the second reduction step is a much simpler case to analyze. In that case, the sole factor that dictates the observed voltammetric response is the relative magnitude of the structural relaxation energy with respect to the difference between the two semi-adiabatic reduction potentials.

In both classical and inverted potential systems, ion pairing of the reduction products with alkali metal counterions decreases the potential difference between the first and second electron-addition reactions. This effect occurs because coordination of the cations to the mononanion, [KA], increases the electron affinity in comparison to A^{-} , and the second ion-pairing energy

($K^{+} + [KA]^{-1} \rightarrow [K_2A]$) to the more electron rich $[KA]^{-1}$ is more favorable than the first.

To fully understand the voltammetric behavior of multielectron redox systems the relative changes of the total energy as a function of solvation, structural relaxation, and ion pairing must be combined. The theoretical square scheme analysis method presented herein should have general utility in deconvolving the relationship between structure and redox potential of molecules as expressed in their voltammetric behavior.

Acknowledgment. This work was supported in part by the National Science Foundation. M.-H.B. thanks the UNC Chemistry Department for the J. T. Dobbins fellowship. We gratefully acknowledge the North Carolina Supercomputing Center for providing computational time and technical assistance, and we thank the reviewers for helpful comments.

Supporting Information Available: Coordinates for optimized geometries of all calculations reported herein, calculated vibrational frequencies of all systems, and itemized energies (PDF). This material is available free of charge via the Internet at <http://pubs.acs.org>.

JA016905+